

Neuron, Volume 95

Supplemental Information

**Origins of Cell-Type-Specific Olfactory Processing
in the *Drosophila* Mushroom Body Circuit**

Kengo Inada, Yoshiko Tsuchimoto, and Hokto Kazama

CONTENTS

Figure S1 (related to Figure 1)	PN and KC responses to activation of <i>VT33006-Gal4</i> -positive PNs with two-photon optogenetics
Figure S2 (related to Figure 1)	Integration of multiple PN inputs in KCs
Figure S3 (related to Figure 3)	KC responses to optogenetic activation and ACh iontophoresis
Figure S4 (related to Figure 4)	KC-type-specific recruitment of inhibition via APL neurons requires spiking activity
Table S1 (related to Figure 1)	List of <i>VT33006-Gal4</i> -positive glomeruli
Table S2 (related to STAR Methods)	List of genotypes used in the study

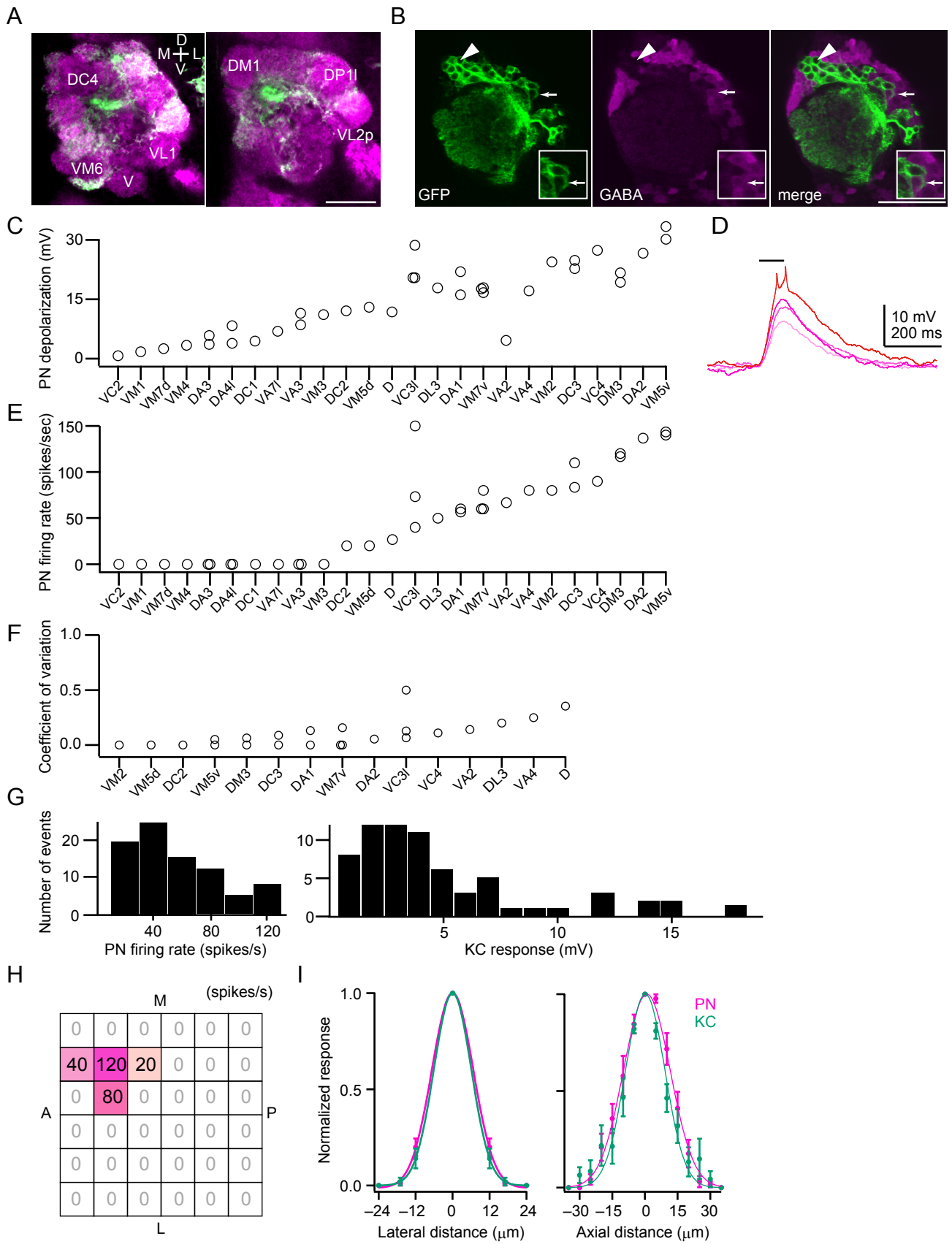


Figure S1 (related to Figure 1). PN and KC responses to activation of *VT33006-Gal4*-positive PNs with two-photon optogenetics

- (A) Confocal images of the immunostained antennal lobe taken at different planes along the anterior-posterior axis. Magenta, nc82 (neuropil), green, anti-GFP. *VT33006-Gal4* labels ~44 antennal lobe glomeruli. The identities of Gal4-negative glomeruli are indicated in white. D, dorsal, V, ventral, L, lateral, M, medial. Scale bar, 20 μm .
- (B) Immunostaining against GABA (magenta). Scale bar, 50 μm . Most of the *VT33006-Gal4*-positive cells are immunonegative for GABA (arrowhead) and only a small number of them are immunopositive (arrow, inset; 9.3 ± 1.1 cells per hemisphere, $n = 3$ flies). Furthermore, this Gal4 line labels the medial antennal lobe tract strongly (data not shown). These results together suggest that most of the *VT33006-Gal4*-positive cells are PNs.
- (C) Peak depolarization in ReaChR-expressing PNs upon two-photon excitation of single ROIs. Depolarization was observed in all the 25 *VT33006-Gal4*-positive glomeruli tested ($n = 36$ PNs). Each dot corresponds to data from a single PN.
- (D) Stimulation with stronger laser power made PNs spike (example responses in glomerulus VM3, stimulation at 8, 10, 11, and 14 mW). Black bar, IR stimulation.
- (E) Spikes were evoked in 15 out of 25 *VT33006-Gal4*-positive glomeruli tested (60%, $n = 36$ PNs) in response to IR stimulation at the laser power employed for examining the integration of multiple synaptic inputs in KCs. Each dot corresponds to data from a single PN.
- (F) Coefficient of variation was calculated from data shown in (E) to quantify the trial-to-trial variability of PN spiking responses. Low coefficient of variation in most of the glomeruli indicates that IR stimulation drives PNs reliably.
- (G) Histograms of the PN spiking response (left) and the KC response (right) evoked by single ROI stimulation. Firing rate was calculated in 50-ms bins overlapped by 25 ms. Values are peak activity during IR stimulation. $n = 81$ ROIs from 11 PNs and 67 ROIs from 9 KCs.
- (H) Sample PN activity evoked by IR stimulation of each ROI. A, anterior, P, posterior, L, lateral, M, medial.
- (I) Relationship between normalized PN/KC responses and the lateral (x- and y- axes) distance (left) or the axial (z-axis) distance (right) from the most effective ROI. Solid lines are Gaussian fits. A positive axial distance corresponds to a dorsal shift. For the lateral distance, the full width at half maximum is 15.8 μm for PNs and 14.2 μm for KCs. For the axial distance, the full width at half maximum is 25.7 μm for PNs and 19.4 μm for KCs. $n = 11$ PNs and 9 KCs. The chance of simultaneously stimulating two neighboring glomeruli presynaptic to our set of recorded KCs was likely low, because both lateral and axial resolutions of KC responses matched with those of PN spikes. If multiple PNs in neighboring glomeruli were activated by the stimulation of each ROI, the resolution of KC responses would have been much worse than that of PN spikes.

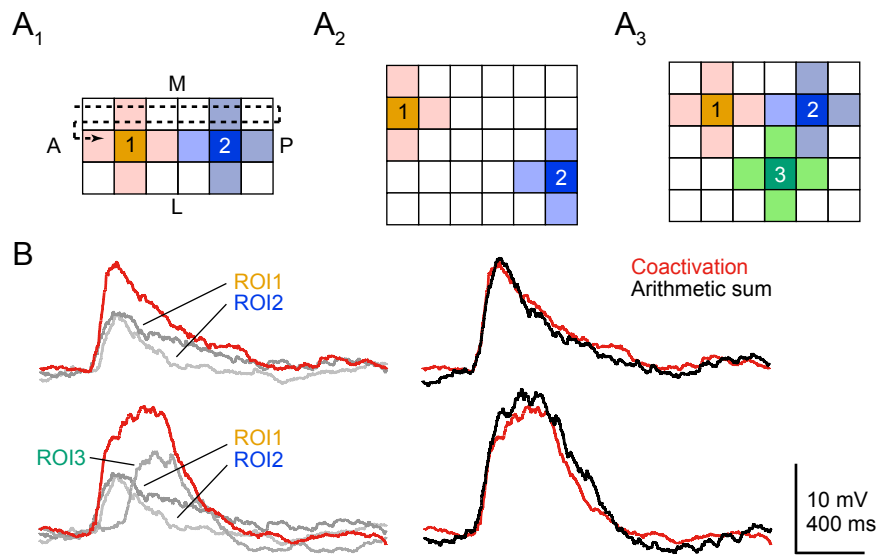


Figure S2 (related to Figure 1). Integration of multiple PN inputs in KCs

(A) Examples of stimulation patterns used to examine the integration of inputs from two (A_1 and A_2) or three (A_3) ROIs in KCs. See STAR Methods for the criteria for selecting the ROIs. A, anterior, P, posterior, L, lateral, M, medial. Arrow indicates the scan direction. Scan speed along A-P axis is shorter than that for M-L axis.

(B) KC responses (average across three trials) to combinations of ROIs shown in A_3 .

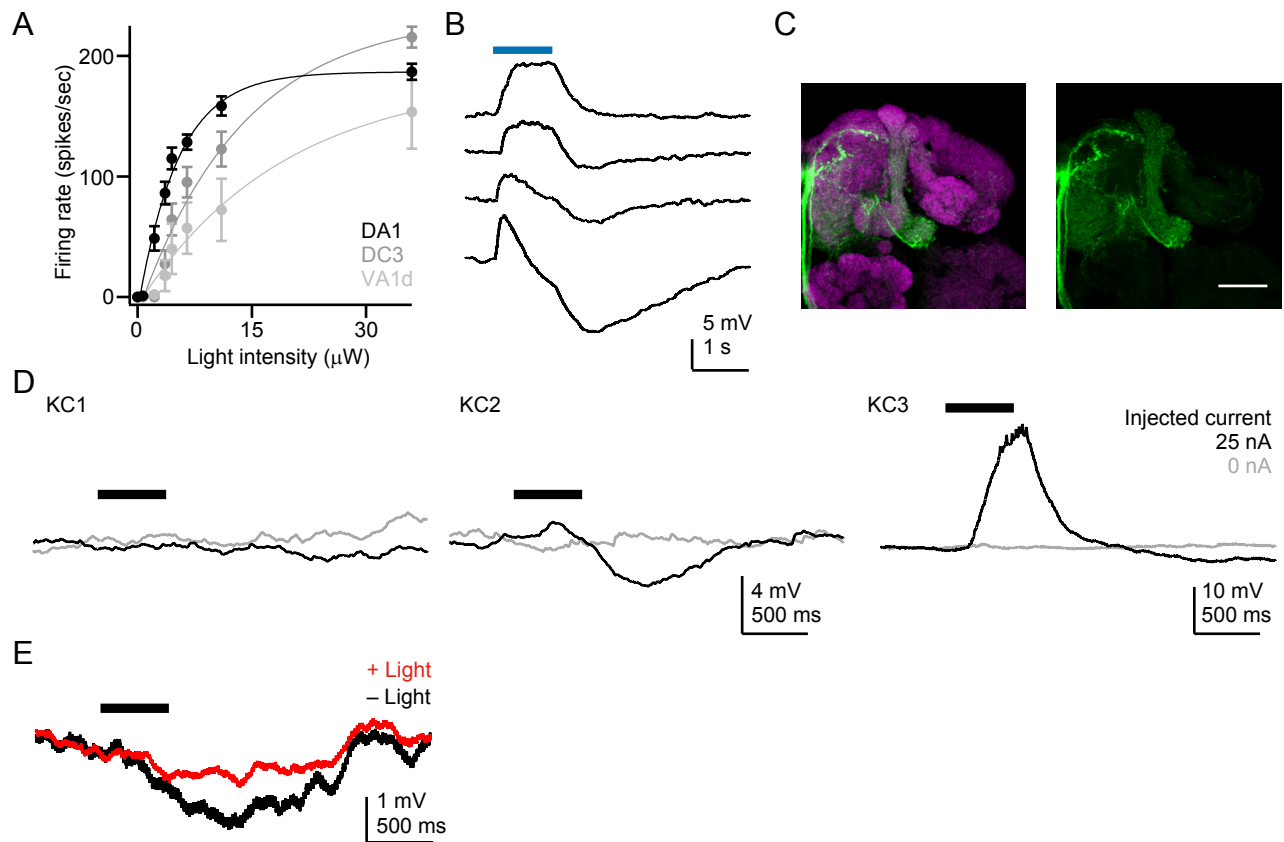


Figure S3 (related to Figure 3). KC responses to optogenetic activation and ACh iontophoresis

- (A) Relationship between *Mz19-Gal4*-positive PN firing rate and LED light intensity in *Mz19-Gal4>ReaChR* flies ($n = 11, 4, 4$ for DA1, DC3 and VA1d PNs, respectively). Firing rate was calculated in 50-ms bins overlapped by 25 ms and averaged across the illumination period (1 s).
- (B) Responses of four different KCs to light in *Mz19-Gal4>ReaChR* flies ($6.5 \mu\text{W}$). Blue bar, light stimulation. Each trace is an average of three trials.
- (C) Left, projection of a confocal stack of a fly brain (neuropil in magenta) expressing *myr::GFP* (green) driven by *APL-Gal4*. Scale bar, $20 \mu\text{m}$. Although GFP signals are found in neurons innervating the superior medial protocerebrum and the crepine (cell bodies are anterior to the spur), importantly, the Gal4 driver does not label cells other than APL neurons in the MB (Wu et al., 2013). Right, GFP channel.
- (D) Representative KC responses from the same brain to iontophoresis of ACh into the MB calyx. To ensure that the induced inhibition remains local (KC2), we confirmed that some KCs (KC1) in the same brain showed no response under the identical iontophoresis condition. Some KCs under the direct influence of injected ACh showed excitation (KC3). Black bar, current injection.
- (E) Representative KC responses to ACh iontophoresis in the calyx in a fly expressing Arch in APL neurons with (red) or without (black) optical stimulation. Each trace is an average of three trials. Light was applied continuously throughout the response period. Black bar, current injection for ACh iontophoresis (500 ms). Optical suppression of APL neuron decreases the amount of inhibition evoked by ACh iontophoresis.

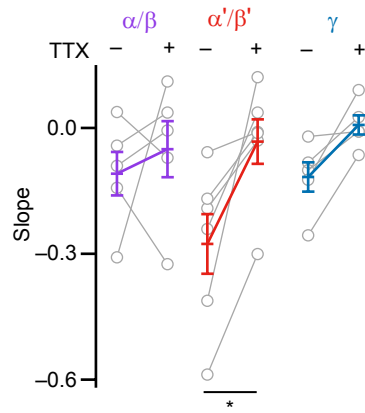


Figure S4 (related to Figure 4). KC-type-specific recruitment of inhibition via APL neurons requires spiking activity

Relationship between the mean KC membrane potential during current injection and the offset response measured 500 ms after the end of current injection. The slope was calculated by performing a linear fit separately to data from each KC types as in Figure 4C ($n = 5, 6, 5$ for α/β , α'/β' , and γ KCs, respectively). The slope for α'/β' KCs was significantly decreased by the addition of tetrodotoxin (TTX; $*p < 0.05$, paired t-test with Bonferroni correction). The slope for α'/β' KCs after application of tetrodotoxin was not significantly different from zero ($p > 0.60$, t-test).

Table S1 (related to Figure 1). List of VT33006-Gal4-positive glomeruli
 The list of glomeruli labeled by VT33006-Gal4 (indicated with an open circle).

Glomerulus	VT33006	Glomerulus	VT33006
D	O	V	
DA1	O	VA1d	O
DA2	O	VA1v	O
DA3	O	VA2	O
DA4l	O	VA3	O
DA4m	O	VA4	O
DC1	O	VA5	O
DC2	O	VA6	O
DC3	O	VA7l	O
DC4		VA7m	O
DL1	O	VC1	O
DL2d	O	VC2	O
DL2v	O	VC3l	O
DL3	O	VC3m	O
DL4	O	VC4	O
DL5	O	VL1	
DM1		VL2a	O
DM2	O	VL2p	
DM3	O	VM1	O
DM4	O	VM2	O
DM5	O	VM3	O
DM6	O	VM4	O
DP1l		VM5d	O
DP1m	O	VM5v	O
		VM6	
		VM7d	O
		VM7v	O

Table S2 (related to STAR Methods). List of genotypes used in the study
The genotypes of flies used in the study.

Figure	Genotype
Figure 1B	<i>UAS-myr::GFP (attP40)/+; VT33006-Gal4 (attP2)/UAS-myr::GFP (attP2)</i>
Figures 1D, F-I	<i>UAS-ReaChR::Citrine (attP40)/+; VT33006-Gal4 (attP2)/+</i>
Figures 3B, D-F	<i>Mz19-Gal4, UAS-ReaChR::Citrine (attP40); +</i>
Figure 3H	<i>UAS-Archaerhodopsin-3::GFP (attP40); APL-Gal4</i>
Figures 4B-D	<i>Mz19-Gal4, UAS-mCD8GFP::GFP (attP40)/UAS-CsChrimson::mVenus (attP40) (*), or UAS-Archaerhodopsin-3::GFP (attP40); APL-Gal4</i>
Figure 4E	<i>UAS-Archaerhodopsin-3::GFP (attP40); APL-Gal4</i>
Figures 5B-E	<i>UAS-CsChrimson::mVenus (attP40); VT43924-Gal4 (attP2)</i>
Figures 6C-E	<i>UAS-GCaMP6s (attP40); VT43924-Gal4 (attP2), UAS-GCaMP6s (VK00005)</i>
Figures 7A-D	<i>UAS-GCaMP5G (attP40); +; OK107-Gal4</i>
Figures 8A-E	<i>UAS-GCaMP5G (attP40); +; OK107-Gal4</i>
Figures S1A, B	<i>UAS-myr::GFP (attP40)/+; VT33006-Gal4 (attP2)/UAS-myr::GFP (attP2)</i>
Figures S1C-I	<i>UAS-ReaChR::Citrine (attP40)/+; VT33006-Gal4 (attP2)/+</i>
Figure S2B	<i>UAS-ReaChR::Citrine (attP40)/+; VT33006-Gal4 (attP2)/+</i>
Figures S3A, B	<i>Mz19-Gal4, UAS-ReaChR::Citrine (attP40); +</i>
Figure S3C	<i>UAS-myr::GFP (attP40); APL-Gal4/ UAS-myr::GFP (attP2)</i>
Figures S3D, E	<i>UAS-Archaerhodopsin-3::GFP (attP40); APL-Gal4</i>
Figure S4	<i>Mz19-Gal4, UAS-mCD8GFP::GFP (attP40)/UAS-CsChrimson::mVenus (attP40) (*), or UAS-Archaerhodopsin-3::GFP (attP40); APL-Gal4</i>

(*) Without provision of ATR.